ChemPubSoc Europe

DOI: 10.1002/ejic.201701154

EurJIC European Journal of Inorganic Chemistry

Full Paper

Nitrogen-Rich Lanthanide Complexes

Rare-Earth Complexes with the 5,5′-Bitetrazolate Ligand – Synthesis, Structure, Luminescence Properties, and Combustion Catalysis

Gleb A. Chesnokov,[a] Maxim A. Topchiy,[a,b] Andrey F. Asachenko,[a,b,c] Nikita V. Muravyev,[d] Leonid I. Grishin,[d,e] Anna S. Nikiforova,[d] Valentina V. Utochnikova,[a,f] Victor B. Rybakov,[a] Victor N. Khrustalev,[c] and Mikhail S. Nechaev*[a,b]

Abstract: A complete series of complexes of the lanthanides and yttrium (except radioactive Pm) with the 5,5′-bitetrazolate (BT^{2-}) ligand were synthesized from sodium 5,5′-bitetrazolate and available rare-earth (RE) salts. Eight new complexes were structurally characterized by single-crystal XRD. The $[M(BT)(H_2O)_7]_2[BT]\cdot 6H_2O$ [M = Pr (**1**), Gd (**2**)] complexes are isomorphous and consist of $[M(BT)(H_2O)_7]^+$ ions in which only one BT^{2-} ligand acts as a chelate for each metal center. The complexes $[M(H_2O)_8]_2[BT]_3\cdot 4H_2O$ [M = Y (**3**), Dy (**4**), Ho (**5**), Tm (**6**), Yb (**7**), Lu (**8**)] are saltlike compounds that do not exhibit any significant metal–nitrogen contacts. Luminescence was very informative for the determination of the number of inner-sphere coordinated water molecules in the solid samples. Despite its low luminescence intensity owing to its high hydrate composition, the deuterated europium complex exhibited an internal quantum yield of 44 %. The catalytic activities of the 5,5′-bitetrazolate salts for the decomposition and combustion reactions of energetic materials were tested. Although no effect was found for nitramine (HMX) explosive, the impact of the salts on the thermolysis of ammonium perchlorate (AP) was established. The addition of 5 % $[Dy(H_2O)_8]_2[BT]_3\cdot 4H_2O$ decreases the temperature at the maximum reaction rate by 100 °C. The catalytic effect during combustion is apparently masked by the inhibitory influence of water; however, for $[Pr(BT)(H_2O)_7]_2[BT]\cdot 6H_2O$, a 20 % increase in the AP burning rate was observed.

1. Introduction

Nitrogen-rich N-heterocyclic ligands, such as tetrazoles, are of high fundamental interest. Their complexes can serve as high-energy materials[1] or nitrogen-generating agents.[1b,2] Surprisingly, in spite of the interesting properties of the tetrazole group, the chemistry of lanthanides with tetrazole-based ligands is much less developed. In addition to energetic applications, lanthanide complexes with nitrogen-rich ligands have potential applications as light-emitting dopants in two main domains, namely, (1) optical and electro-optical devices, including laser materials, amplifiers, and organic light-emitting diodes (OLEDs)[3] and (2) biomedical analysis.[4]

There is only one report on rare-earth (RE) complexes of the 5,5′-bitetrazole dianion (BT^{2-}). Eulgem et al. synthesized seven $Ln_2(BT)_3\cdot nH_2O$ complexes.[5] The XRD analysis of the molecular structures of the BT complexes revealed three different structural types and a decreasing tendency to coordinate the BT^{2-} ligand as the rare-earth ion varied from La to Er: (1) for La and Ce, $[Ln_2(BT)_3(H_2O)_{12}]\cdot 2H_2O$ formed; (2) for Nd, Sm, and Eu, $[Ln(BT)(H_2O)_7]_2(BT)\cdot 6H_2O$ formed; and (3) for Tb and Er, $[Ln(H_2O)_8]_2(BT)_3\cdot 4H_2O$ formed. This tendency is in full agreement with the decreasing ionic radii along this series and the increasing Lewis acid character (manifested by the increasing hydration enthalpy), which allows coordination compounds for the early Ln elements but favors saltlike compounds for the heavier analogues. However, several questions remain. First, where is the border between the molecular structures of the complexes and salts of rare-earth elements (REEs) with the BT^{2-} ligand? Which structural types correspond to $Pr_2(BT)_3\cdot nH_2O$ and $Gd_2(BT)_3\cdot nH_2O$? Is there a fourth structural type of crystals in a series of heavy rare-earth elements (HREEs, yttrium REE)? To answer these questions, it was decided to synthesize the missing REE complexes with BT^{2-} and characterize their structures.

It is of interest to study the structure–property relationship in the complete series of lanthanide BT complexes in such aspects as luminescence and thermal analysis and to study their properties in combustion catalysis.

[a] *Lomonosov Moscow State University, 1/3 Leninskie Gory, Moscow 119991, Russian Federation*
E-mail: m.s.nechaev@org.chem.msu.ru
https://istina.msu.ru/profile/MikhailSNechaev/
[b] *A. V. Topchiev Institute of Petrochemical Synthesis, Russian Academy of Sciences, Leninsky Prospect 29, Moscow, 119991, Russia*
[c] *Department of Inorganic Chemistry, Peoples' Friendship University of Russia, Miklukho-Maklay Street 6, Moscow, 117198, Russia*
[d] *Semenov Institute of Chemical Physics, Russian Academy of Sciences, 4 Kosygin Str., Moscow 119991, Russian Federation*
[e] *National Research Nuclear University "MEPhI", 31 Kashirskoe Sh., Moscow 115409, Russian Federation*
[f] *Lebedev Physical Institute, Russian Academy of Sciences, 59 Leninsky Prosp., Moscow 119991, Russian Federation*

Supporting information and ORCID(s) from the author(s) for this article are available on the WWW under https://doi.org/10.1002/ejic.201701154.

The differences in their crystal structures makes the study of their luminescence properties fundamentally interesting. Therefore, the difference in the number of coordinated ligands in the terbium and europium complexes may help us to understand their role in the process of lanthanide sensitization. As the hydrate composition influences the luminescence properties, luminescence spectroscopy can be used as a probe to determine the number of inner-sphere water molecules in the complexes.

Ammonium perchlorate (AP) and cyclotetramethylenetetranitramine (HMX), which are a solid oxidizer and an explosive, respectively, are the main components in modern energetic compositions.[6] Although the tailoring of the dependency of the burning rate on the pressure for AP-based systems through the use of catalysts is the subject of many reports,[7] the search for an effective additive is still relevant, and metal salts are effective catalysts for the combustion of AP.[7a,8] The main catalytic agents are supposed to be a metal ion or a metal oxide, both of which form through salt decomposition before the AP thermolysis. Recently, metal salts with high nitrogen contents were proposed as additives in energetic formulations (1) to bring additional energy through the decomposition of the energetic salt and (2) to introduce the catalytic metal ion or compound after the decomposition.[9]

Thus, in the present study, we investigated the synthesis and structure–property relationships of the complete series of lanthanide BT complexes. A general method for the synthesis of rare-earth 5,5′-bitetrazolates is proposed, and the synthesized salts were characterized thoroughly by X-ray diffraction analysis. The luminescence properties of the 5,5′-bitetrazolate salts were also studied. The thermal stabilities of these compounds alone and in mixtures with common energetic materials were investigated, and they showed promising catalytic properties.

2. Results and Discussion

2.1 Synthesis of BT Complexes

The only currently described method for the synthesis of rare-earth 5,5′-bitetrazolates is the reaction of RE sulfates and the barium salt of 5,5′-bitetrazole (Scheme 1).[5] Trivalent lanthanide sulfate and 5,5′-barium bitetrazolate are dissolved in hot water, and the resulting precipitated barium sulfate is removed by filtration. The filtrate is evaporated to dryness, and the solid residue is recrystallized from a minimum amount of water.

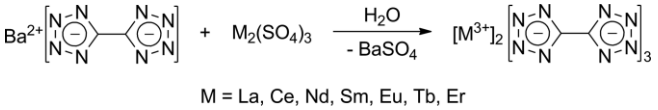

Scheme 1.

We modified this method for the synthesis of rare-earth 5,5′-bitetrazolates. Hydrates of the rare-earth 5,5′-bitetrazolates were synthetized from sodium 5,5′-bitetrazolate and available rare-earth chlorides, nitrates, or acetates (Scheme 2).

General Method for the Synthesis of Rare-Earth 5,5′-Bitetrazolates

Through this synthetic approach, we prepared seven previously described lanthanide 5,5′-bitetrazolates (M = La, Ce, Nd, Sm, Eu, Tb, Er)[5] as well as seven more lanthanide 5,5′-bitetrazolates [M = Pr (**1**), Gd (**2**), Dy (**4**), Ho (**5**), Tm (**6**), Yb (**7**), Lu (**8**)] and yttrium 5,5′-bitetrazolate [M = Y (**3**)], which have not been described previously.

Through the reaction of concentrated aqueous solutions of Na_2BT and $Ho(NO_3)_3$, we obtained small pink crystals and some pink solid. The recrystallization of this mixture from hot water and storage for 2 d afforded pink crystals of the composition $[Ho(H_2O)_8]_2[BT]_3{\cdot}4H_2O$ (**5**). If **5** is heated in vacuo, it loses water up to a decomposition temperature of ca. 350 °C. At this temperature, explosion had not occurred. All other 5,5′-bitetrazolates (**1**–**4** and **6**–**8**) were obtained in a similar manner through the reactions of Na_2BT with $MX_3{\cdot}nH_2O$ in water to give the products in 64–81 % yields. We obtained X-ray-quality crystals of **1**–**8**. On the basis of the XRD data, the composition of the 5,5′-bitetrazolates in the solid state is $[M(BT)_x(H_2O)_m]_2[BT]_y{\cdot}nH_2O$ ($x + y = 3$, $2m + n = 20$; $x = 1$, $y = 2$, $m = 7$, $n = 6$ for M = Pr, Gd; $x = 0$, $y = 3$, $m = 8$, $n = 4$ for M = Y, Dy, Ho, Tm, Yb, Lu).

2.2 XRD Analysis

Compounds **1**–**8** were characterized by single-crystal X-ray diffraction. Their structures are shown in Figures 1, 2, S1, and S2 (Supporting Information) along with the atom-numbering schemes. The full geometric parameters for **1**–**8** are available in the Supporting Information.

Compounds **1**–**8** crystallize in the triclinic space group $P\bar{1}$ and exhibit two different structural types, which were observed previously for the analogous complexes of neodymium, samarium, and europium (type I) and terbium and erbium (type II).[5]

Complexes **1** and **2** (type I) consist of $[M(BT)(H_2O)_7]^+$ cations and BT^{2-} anions {$[M(BT)(H_2O)_7]_2[BT]{\cdot}6H_2O$, M = Pr (**1**) and Gd

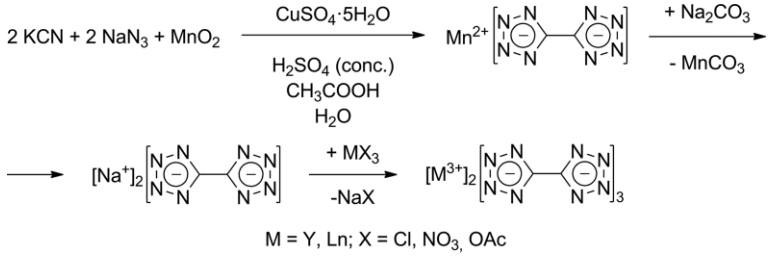

Scheme 2.

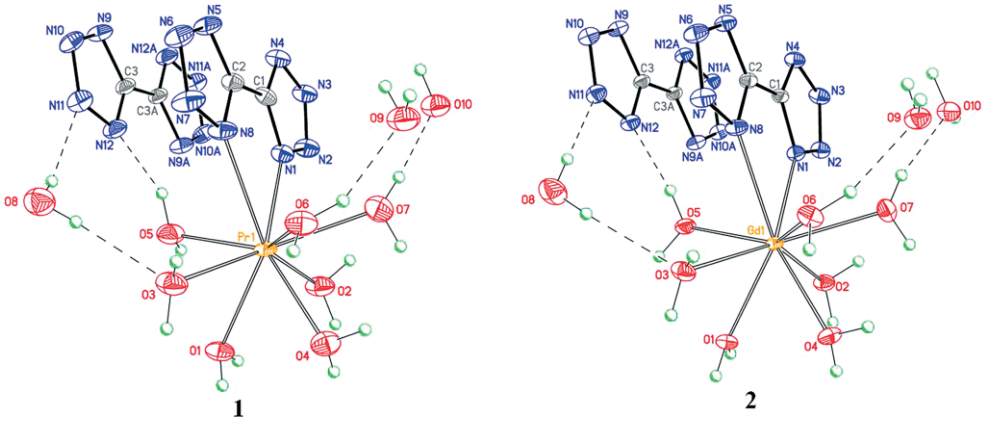

Figure 1. Molecular structures of **1** and **2** (structural type I). The A labels denote symmetrically equivalent atoms. The dashed lines indicate the O–H···N and O–H···O hydrogen bonds.

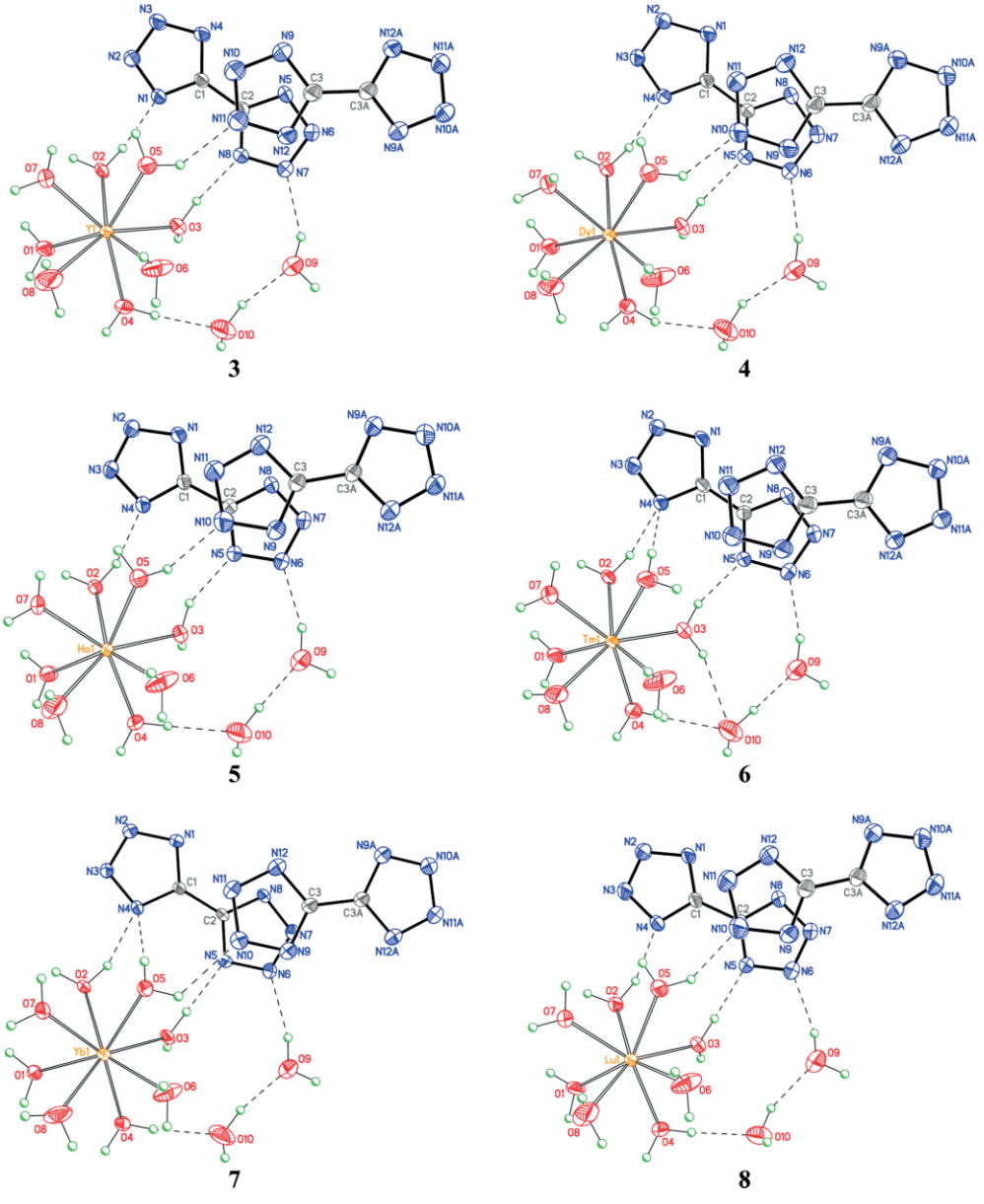

Figure 2. Molecular structures of **3**–**8** (structural type II). The A labels denote symmetrically equivalent atoms. The dashed lines indicate the O–H···N and O–H···O hydrogen bonds.

(**2**), Figure 1}. In the cations, one BT ligand is coordinated to the rare-earth ion in a chelate fashion through the nitrogen atoms at the 1- and 1′-positions (N1 and N8) of the tetrazole rings. Additionally, seven water molecules coordinate to form a distorted tricapped trigonal prism, which represents a typical ninefold coordination for these metal centers. The M–O [2.440(4)–2.556(4) Å in **1** and 2.373(2)–2.488(2) Å in **2**] and M–N bond lengths [2.654(4) and 2.722(4) Å in **1** and 2.584(2) and 2.675(2) Å in **2**] are consistent with the effect of the lanthanoid contraction. The isolated BT^{2-} anion occupies a special position on the inversion center and, thus, possesses intrinsic C_i symmetry. The two $[M(BT)(H_2O)_7]^+$ cations and the BT^{2-} anion form the supramolecular structure through π–π stacking interactions between the coordinated and isolated BT units as well as intermolecular O–H···N hydrogen bonds (Figure S1). The molecular complexes are bound to each other to form a three-dimensional framework through intermolecular O–H···N and O–H···O hydrogen bonds between the solvate water molecules.

Structural type II is represented by **3**–**8**, which consist of $[M(H_2O)_8]^{3+}$ cations and BT^{2-} anions {$[[M(H_2O)_8]_2[BT]_3{\cdot}4H_2O$; M = Y (**3**), Dy (**4**), Ho (**5**), Tm (**6**), Yb (**7**) and Lu (**8**); Figure 2}. The rare-earth ions in **3**–**8** are coordinated by eight water molecules in a distorted square-antiprismatic coordination geometry. The Lu–O bond lengths of 2.291(4)–2.388(4) Å for **8** are noticeably shorter than the Ln–O bond lengths in the other complexes of this structural type and, therefore, reflect the fact that lutetium is the last element of the lanthanide row. The BT^{2-} anions in **3**–**8** form zigzag-like chains along the *c* axis through π–π stacking interactions (Figure S2). The $[M(H_2O)_8]^{3+}$ cations and BT^{2-} anions in **3**–**8** are bound to each other through intermolecular O–H···N and O–H···O hydrogen bonds through the solvate water molecules to form a three-dimensional framework. Interestingly, the small differences in the molecular geometries of **3**–**8** give rise to different hydrogen-bonding systems (Figure 2).

The structural data for the rare-earth $[M_2(BT)_3]{\cdot}nH_2O$ complexes are summarized in Table 1. In agreement with previous results,[5] there are two types of RE complexes with BT^{2-} ligands. The complexes of the light rare-earth elements (LREEs, La to Gd), which are characterized by ionic radii between 1.216 and 1.107 Å (R^{theor}) and hydration enthalpies (ΔH_{hydr}) between –3238 and –3570 kJ/mol, tend to incorporate the "soft" BT^{2-} ligand into their coordination spheres (type I). The La and Ce complexes have the BT^{2-} ligand coordinated in a chelate fashion, and one BT^{2-} ligand bridges two metal atoms to form a $Ln_2(BT)_3$ moiety. The remaining LREEs from Pr to Gd bear only one chelating BT^{2-} ligand in their coordination spheres, and the third BT^{2-} anion is coordinated to water molecules through hydrogen bonds. In all cases, the coordination number of the metal center is nine. The more Lewis acidic HREE cations form saltlike (type II) structures. The ionic radii of the HREEs are below 1.019 Å; correspondingly, their hydration enthalpies lie in the range from –3583 to –3760 kJ/mol. Thus, "hard" water substitutes "soft" BT^{2-} in the coordination sphere. The smaller ionic radii of the HREEs lead to a decrease of the coordination number of the metal ion from nine to eight. All of the BT^{2-} ligands in the type II structures bridge HREE aqua complexes through hydrogen bonds.

2.3 Luminescence Properties

The terbium and europium complexes do not exhibit any remarkable luminescence, as could be predicted on the basis of the large number of quenching water molecules (seven in the terbium coordination sphere and eight in the europium coordination sphere). Nevertheless, the differences in their crystal structures, that is, the different hydrate compositions and the presence or absence of the coordinated ligand, make the study of their luminescence properties fundamentally interesting. Indeed, the Förster and Dexter energy-transfer rates are both sensitive to the donor–acceptor distance (in the present case, the ligand–lanthanide distance), and a comparison of the ratio of through-ligand to through-metal excitation of terbium and eu-

Table 1. Structural type of $[Ln_2(BT)_3]{\cdot}nH_2O$ versus ionic radius (R^{theor}) and hydration enthalpy (ΔH_{hydr}).[5]

M	Compound	CN[a]	BT^{2-} ligands in coordination sphere	R^{theor} [Å][b]	$\Delta H_{hydr.}$ [kJ/mol]
LREEs[c]					
La	$[La_2(BT)_3(H_2O)_{12}]{\cdot}2H_2O$	9	1.5	1.216	–3238
Ce	$[Ce_2(BT)_3(H_2O)_{12}]{\cdot}2H_2O$	9	1.5	1.196	–3370
Pr	$[Pr(BT)(H_2O)_7]_2[BT]{\cdot}6H_2O$	9	1	1.179	–3413
Nd	$[Nd(BT)(H_2O)_7]_2[BT]{\cdot}6H_2O$	9	1	1.163	–3442
Sm	$[Sm(BT)(H_2O)_7]_2[BT]{\cdot}6H_2O$	9	1	1.132	–3515
Eu	$[Eu(BT)(H_2O)_7]_2[BT]{\cdot}6H_2O$	9	1	1.120	–3547
Gd	$[Gd(BT)(H_2O)_7]_2[BT]{\cdot}6H_2O$	9	1	1.107	–3571
HREEs[d]					
Y	$[Y(H_2O)_8]_2[BT]_3{\cdot}4H_2O$	8	0	1.019	–3583,[10] –3594,[11] –3620[12]
Tb	$[Tb(H_2O)_8]_2[BT]_3{\cdot}4H_2O$	8	0	1.04	–3605
Dy	$[Dy(H_2O)_8]_2[BT]_3{\cdot}4H_2O$	8	0	1.027	–3637
Ho	$[Ho(H_2O)_8]_2[BT]_3{\cdot}4H_2O$	8	0	1.015	–3667
Er	$[Er(H_2O)_8]_2[BT]_3{\cdot}4H_2O$	8	0	1.004	–3691
Tm	$[Tm(H_2O)_8]_2[BT]_3{\cdot}4H_2O$	8	0	0.994	–3717
Yb	$[Yb(H_2O)_8]_2[BT]_3{\cdot}4H_2O$	8	0	0.985	–3739
Lu	$[Lu(H_2O)_8]_2[BT]_3{\cdot}4H_2O$	8	0	0.977	–3760

[a] Coordination number. [b] Theoretical ionic radius calculated for the corresponding CN.[13] [c] Light rare-earth elements: Sc, La, Ce, Pr, Nd, Pm, Sm, Eu, and Gd; also known as the cerium group. [d] Heavy rare-earth elements: Y, Tb, Dy, Ho, Er, Tm, Yb, and Lu; also known as the yttrium group.

ropium luminescence might establish the critical ligand–metal distance that still allows ligand-to-metal energy transfer.

Before we studied the luminescence properties of $[Tb(H_2O)_8]_2[BT]_3{\cdot}4H_2O$ and $[Eu(BT)(H_2O)_7]_2[BT]{\cdot}6H_2O$, we ensured that the ligand triplet-state energy was suitable for sensitization to occur. The room-temperature and 77 K spectra of $[Gd(BT)(H_2O)_7]_2[BT]{\cdot}6H_2O$ and $[Lu(H_2O)_8]_2[BT]_3{\cdot}4H_2O$ coincide and consist of a fluorescence band (0–0 transition at λ = 350 nm, band maximum at λ = 400 nm) and a phosphorescence band [no way to determine the 0–0 transition, maximum at λ = 490 nm; excited-state lifetime (5 ± 1) µs], which correspond to excited-state energies of 26400 and 20800 cm^{-1} for S_1 and T_1, respectively (Figure 3). These energies are well within the range of values that provide efficient sensitization for both terbium and europium.

Despite the suitable triplet-state energy, neither the terbium nor the europium luminescence seemed to be sensitized by the BT ligand, and the excitation spectra of $[Tb(H_2O)_8]_2[BT]_3{\cdot}4H_2O$ and $[Eu(BT)(H_2O)_7]_2[BT]{\cdot}6H_2O$ show almost pure ionic bands (Figure 4). The absence of ligand-to-metal energy transfer is also indicated by the presence of the ligand band in the spectra of both $[Tb(H_2O)_8]_2[BT]_3{\cdot}4H_2O$ and $[Eu(BT)(H_2O)_7]_2[BT]{\cdot}6H_2O$. The ligand-to-metal luminescence intensity ratio depends on the excitation wavelength (Figure 5), which is consistent with the excitation data measured at the ligand luminescence wavelength (Figure 4).

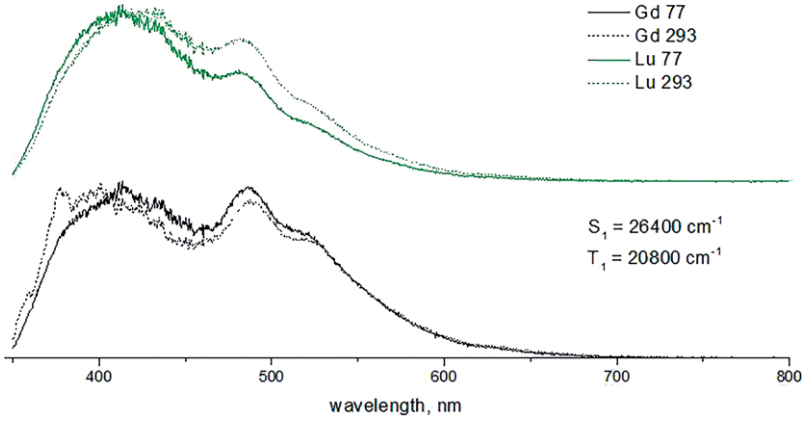

Figure 3. Steady-state luminescence spectra of $[Gd(BT)(H_2O)_7]_2[BT]{\cdot}6H_2O$ and $[Lu(H_2O)_8]_2[BT]_3{\cdot}4H_2O$ (room temperature and 77 K; λ_{ex} = 337 nm).

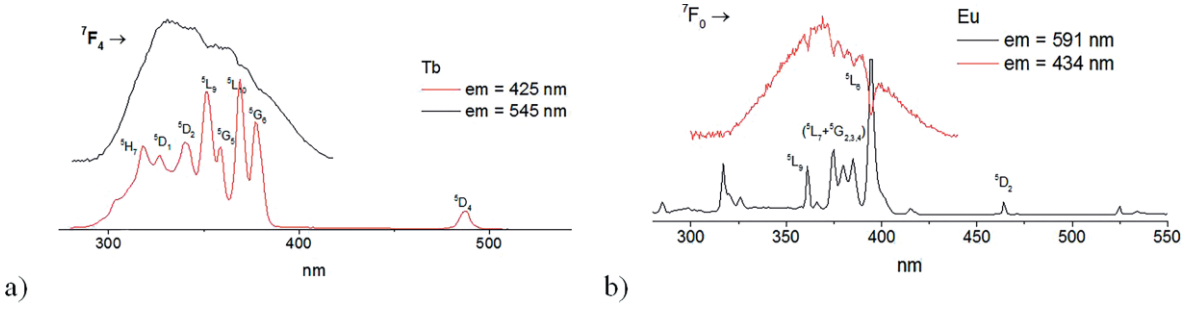

Figure 4. Steady-state excitation spectra of (a) $[Tb(H_2O)_8]_2[BT]_3{\cdot}4H_2O$ and (b) $[Eu(BT)(H_2O)_7]_2[BT]{\cdot}6H_2O$ (room temperature).

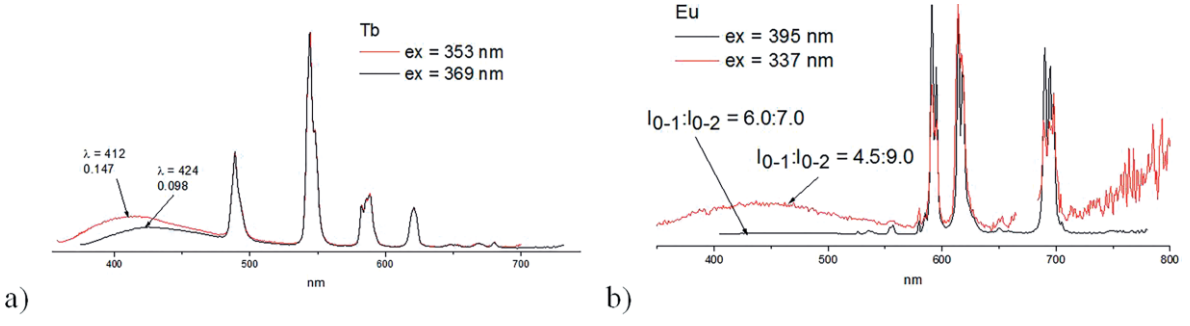

Figure 5. Steady-state emission spectra of (a) $[Tb(H_2O)_8]_2[BT]_3{\cdot}4H_2O$ and (b) $[Eu(BT)(H_2O)_7]_2[BT]{\cdot}6H_2O$ (room temperature).

These facts indicate that the ligand and metal act independently in the terbium and europium complexes, irrespective of the presence or absence of the BT ligand in the first coordination sphere. Surprisingly, in the spectrum of $[Eu(BT)(H_2O)_7]_2[BT]\cdot 6H_2O$, the ratio of the europium bands depends on the excitation wavelength: for excitation through the ligand (λ = 337 nm), the intensity ratio of the $^5D_0$–$^7F_1$ and $^5D_0$–$^7F_2$ transitions is I_{0-1}/I_{0-2} = 1:2, whereas the excitation through the metal ion (λ = 395 nm) leads to I_{0-1}/I_{0-2} = 1:1 (Figure 5). We first suspected that this could be attributed to the presence of two europium atoms with different coordination environments that would be excited at different wavelengths. However, this was not the case: the band corresponding to the europium 0–0 transition (λ = 579 nm) was not split, and this indicates the presence of only one coordination environment for europium (Figure 6).

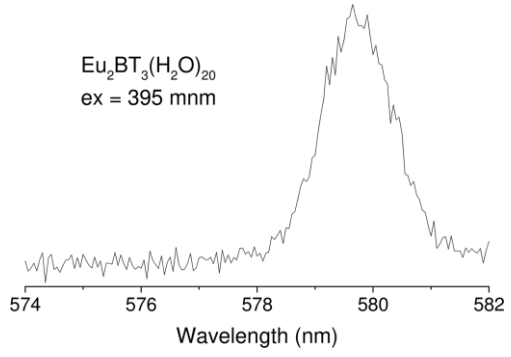

Figure 6. A 0–0 transition in the steady-state emission spectrum of $[Eu(BT)(H_2O)_7]_2[BT]\cdot 6H_2O$ (room temperature).

Despite the previous evidence, this fact together with the presence of ligand-sensitized europium luminescence leads to the conclusion that ligand-to-metal energy transfer does occur but is inefficient. However, metal-to-ligand transfer also leads to a decrease of the $^5D_0$–$^7F_1$ transition intensity.

The low luminescence intensity is attributed to the low energy transfer and also to quenching by the coordinated water molecules. This results in more intense luminescence at 77 K; however the profiles of the spectra were unaffected (Figure 7). To study the influence of the coordinated water molecules in more detail, the analogous deuterated complexes $[Tb(D_2O)_8]_2[BT]_3\cdot 4D_2O$ and $[Eu(BT)(D_2O)_7]_2[BT]\cdot 6D_2O$ were obtained.

The profiles of the excitation (Figure 8) and luminescence spectra were not affected by deuteration, but, as expected, the excited-state lifetimes of the terbium and europium complexes increased dramatically (Figure 9 and Supporting Information). The excited-state lifetimes were independent of the excitation wavelength and the emission band Table 2; therefore, only two examples are given in Figure 9.

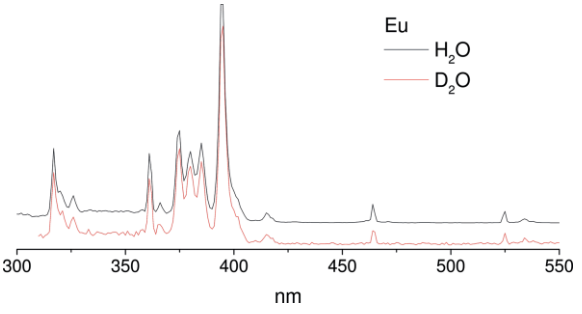

Figure 8. Steady-state excitation spectra of $[Eu(BT)(H_2O)_7]_2[BT]\cdot 6H_2O$ and $[Eu(BT)(D_2O)_7]_2[BT]\cdot 6D_2O$ (room temperature).

From these values (see below), we can calculate the lanthanide quantum yields for the europium complexes, which are the only reasonable values owing to the almost absent ligand-to-metal energy transfer. The pure radiative lifetime of the europium compounds can be calculated from the spectra [Equation (1)].

$$\frac{1}{\tau_{rad}} = 14.65\ s^{-1} \times n^3 \times \frac{I_{tot}}{I_{0-1}} \quad (1)$$

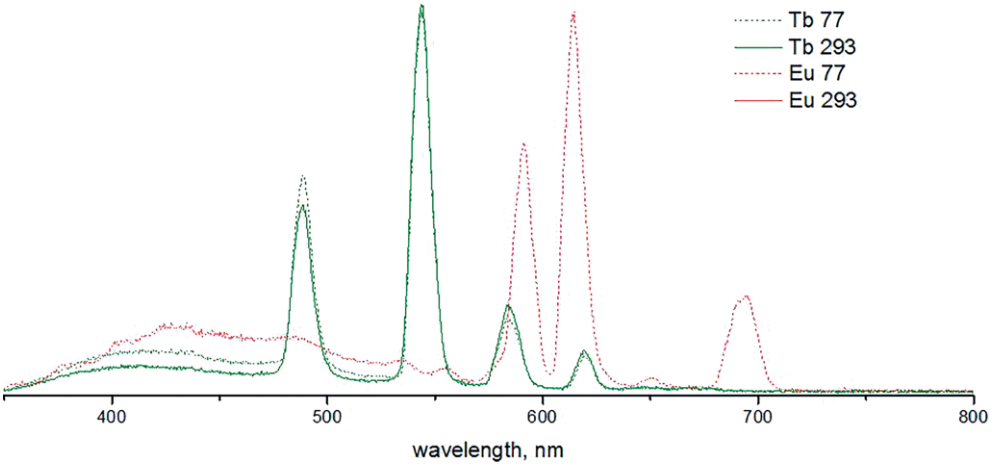

Figure 7. Steady-state emission spectra of (a) $[Tb(H_2O)_8]_2[BT]_3\cdot 4H_2O$ and (b) $[Eu(BT)(H_2O)_7]_2[BT]\cdot 6H_2O$ (room temperature and 77 K).

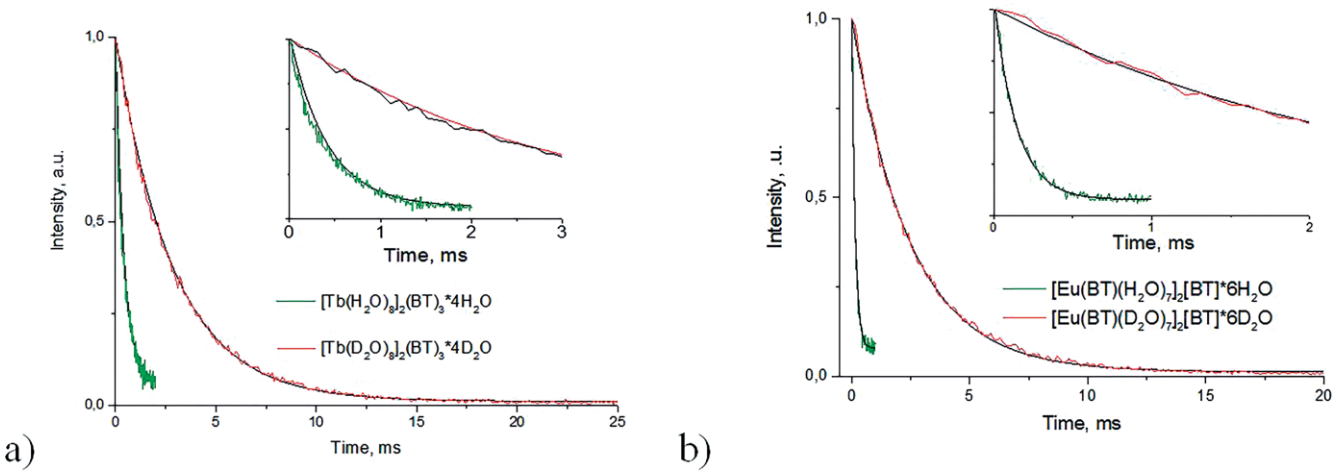

Figure 9. Steady-state luminescence decay curves (room temperature) of (a) $[Tb(H_2O)_8]_2[BT]_3{\cdot}4H_2O$ (λ_{ex} = 369 nm, λ_{em} = 545 nm) and $[Tb(D_2O)_8]_2[BT]_3{\cdot}4D_2O$ (λ_{ex} = 370 nm, λ_{em} = 544 nm); (b) $[Eu(BT)(H_2O)_7]_2[BT]{\cdot}6H_2O$ (λ_{ex} = 337 nm, λ_{em} = 591 nm) and $[Eu(BT)(D_2O)_7]_2[BT]{\cdot}6D_2O$ (λ_{ex} = 395 nm, λ_{em} = 614 nm).

Table 2. Lifetimes [ms] of the excited states of $[Tb(H_2O)_8]_2[BT]_3{\cdot}4H_2O$, $[Tb(D_2O)_8]_2[BT]_3{\cdot}4D_2O$, $[Eu(BT)(H_2O)_7]_2[BT]{\cdot}6H_2O$, and $[Eu(BT)(D_2O)_7]_2[BT]{\cdot}6D_2O$.

Compound	Excitation wavelength [nm]			
	337	337 (λ_{em} = 432 nm)	369	395
$[Tb(H_2O)_8]_2[BT]_3{\cdot}4H_2O$	–	0.006(1)	0.42(1)	–
$[Eu(BT)(H_2O)_7]_2[BT]{\cdot}6H_2O$	0.14(2) (average)	0.005(1)	–	0.14(2)
	0.142(2) (591 nm)			0.152(4) (591 nm)
	0.157(5) (591 nm)			0.150(3) (614 nm)
	0.139(4) (614 nm)			0.103(3) (614 nm)
				0.131(8) (690 nm)
	t_{rad} = 4.0			t_{rad} = 5.3
$[Tb(D_2O)_8]_2[BT]_3{\cdot}4D_2O$	–	–	2.84(1)	–
$[Eu(BT)(D_2O)_7]_2[BT]{\cdot}6D_2O$	–	–	–	2.46(1) (614 nm)
				t_{rad} = 5.65

Therefore, the quantum yield can be calculated from Equation (2)

$$Q_{Ln}^{Ln} = \frac{\tau_{obs}}{\tau_{rad}} \times 100\ \% \quad (2)$$

This value is extremely low (2.6 %) for $[Eu(BT)(H_2O)_7]_2[BT]{\cdot}6H_2O$ and increases to 44 % upon deuteration.

Moreover, the quantity of coordinated water molecules (q) in the internal coordination sphere can be calculated from the lifetime values for both europium and terbium and compared with the experimental data [Equations (3) and (4)].

$$q(Eu) = 1.05 \times \left(\frac{1}{\tau_{H_2O}} - \frac{1}{\tau_{D_2O}}\right) = 7.1 \quad (3)$$

$$q(Tb) = 4.2 \times \left(\frac{1}{\tau_{H_2O}} - \frac{1}{\tau_{D_2O}}\right) = 8.3 \quad (4)$$

This method was established for solutions[14] and has rarely been used for powders.[15] Thus, it is important to determine if the established correlations can also be used for solid samples. The calculations show that the luminescence data can be used to distinguish between seven and eight coordinated molecules and, therefore, can provide information on complex compositions in the absence of structural data.

2.4 Thermal Stabilities

Thermogravimetric studies were performed for the Y, La, Ce, Pr, Sm, Eu, Gd, Dy, Tm, Yb, and Lu complexes. Typical differential scanning calorimetry/thermogravimetry (DSC/TG) scans are presented in Figure 10 for $[Yb(H_2O)_8]_2[BT]_3{\cdot}4H_2O$ (see Figure S9 and S10 for those of the Gd and Y complexes). For all studied bitetrazolate salts, three general stages were observed: (1) a mass loss from 50 to 150 °C with a corresponding endothermal effect on the caloric DSC signal; (2) a second slow mass loss in the range 150–300 °C; (3) a mass loss with a weak exothermal effect in the range 300–500 °C. The mass-loss values for these three regions along with the heat effect and number of endothermic peaks for the first stage of water release are presented in Table 3.

Previously, explosive decomposition was reported for $[Eu(BT)(H_2O)_7]_2[BT]{\cdot}6H_2O$.[5] In the present work, no such behavior was observed. Most probably, this is due to the small amounts of sample (ca. 1 mg) that we used in our tests compared with the 10 mg samples used by Eulgem et al.[5]

A visual comparison of the obtained data for all studied 5,5′-bitetrazolates (Figure 11) reveals that the order of first-stage mass loss (dehydration) in the TG curves is the same as the order of the elements in the periodic table. The temperature corresponding to 5 % mass loss, taken as a measure of this

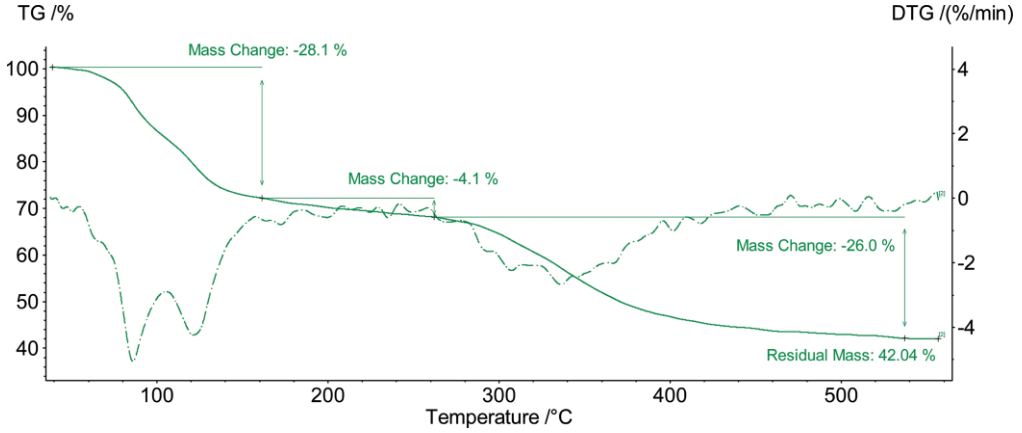

Figure 10. Mass loss (TG) and its derivative (DTG, dashed curve) for $[Yb(H_2O)_8]_2[BT]_3 \cdot 4H_2O$ at a heating rate of 10 K/min in an argon flow.

Table 3. Thermal stability parameters for the studied 5,5′-bitetrazolates.

Sample	First region				Second region	Third region	>550 °C
	Heat effect [J/g]	DSC peaks	Mass loss [%]	$T_{0.05}$ [°C]	Mass loss [%]	Mass loss [%]	Residual mass [%]
$[La_2(BT)_3(H_2O)_{12}] \cdot 2H_2O$	–540	1	24	124	3	25	48
$[Ce_2(BT)_3(H_2O)_{12}] \cdot 2H_2O$	–510	1	24	121	4	27	44
$[Pr(BT)(H_2O)_7]_2[BT] \cdot 6H_2O$	–480	2	22	111	4	26	47
$[Sm(BT)(H_2O)_7]_2[BT] \cdot 6H_2O$	–260	2	24	100	4	24	47
$[Eu(BT)(H_2O)_7]_2[BT] \cdot 6H_2O$	–280	2	19	98	7	25	49
$[Gd(BT)(H_2O)_7]_2[BT] \cdot 6H_2O$	–380	3	23	83	3	24	49
$[Dy(H_2O)_8]_2[BT]_3 \cdot 4H_2O$	–530	2	29	87	4	24	43
$[Tm(H_2O)_8]_2[BT]_3 \cdot 4H_2O$	–360	3	26	84	3	23	48
$[Yb(H_2O)_8]_2[BT]_3 \cdot 4H_2O$	–390	2	28	81	4	26	42
$[Lu(H_2O)_8]_2[BT]_3 \cdot 4H_2O$	–310	2	27	79	2	25	46

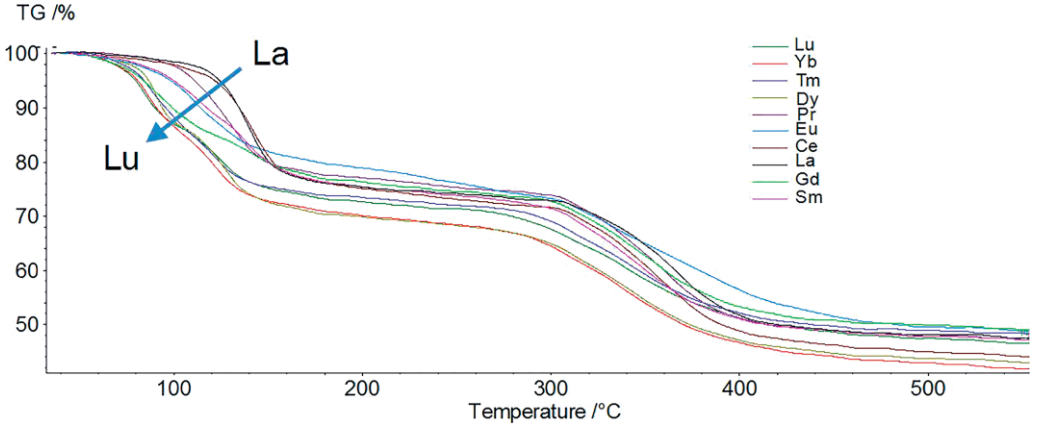

Figure 11. Mass-loss curves for the studied 5,5′-bitetrazolates.

effect, decreases as the atomic number of the lanthanide increases (from 124 °C for La to 79 °C for Lu, Table 3).

2.5 Combustion Catalysis

The friction sensitivities of selected 5,5′-bitetrazolates (La, Sm, and Tm) were determined, and the compounds are insensitive, that is, at a maximal load of 360 N, no explosions were observed over ten runs.[16]

The catalytic activities of the series of lanthanide 5,5′-bitetrazolates for the thermal decomposition of ammonium perchlorate were studied. A comparison of the thermogravimetric (TG) and heat flow (DSC) signals for neat AP and its mixtures with 5 % $[Pr(BT)(H_2O)_7]_2[BT] \cdot 6H_2O$ and 5 % $[Dy(H_2O)_8]_2[BT]_3 \cdot 4H_2O$ is shown in Figure 12. Under linear heating, pure ammonium perchlorate first transforms from the orthorhombic phase to the cubic phase at ca. 240 °C with an endothermal effect. Then, the AP decomposes in two stages (i.e., a low-temperature one and a high-temperature one), in line with the literature data.[17] The addition of as little as 5 wt.-% of the 5,5′-biterazolates to AP significantly affects its decomposition. The second stage of the perchlorate thermolysis shifts to lower tempera-

tures, and both steps merge, as presented in Figure 12 for $[Dy(H_2O)_8]_2[BT]_3{\cdot}4H_2O$. To compare the catalytic activities of the different additives, the temperature value corresponding to the maximal mass loss (T_{max}^{DTG}) was used, as it almost coincides with the temperature of the maximal heat release from the DSC curves. The catalytic activities of the series of lanthanide 5,5′-bitetrazolates are presented in Table 4. The highest catalytic effect is the shift of the second stage of AP decomposition by ca. 100 °C, which was observed for the Y, Dy, Ho, and Er salts.

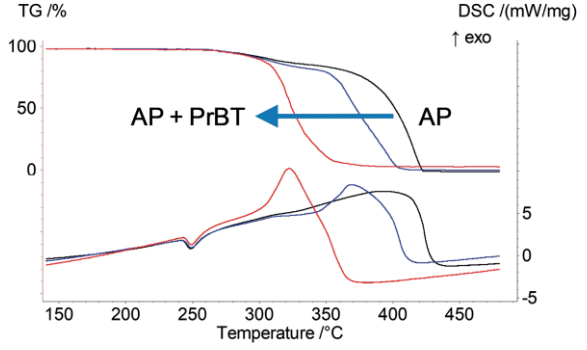

Figure 12. Thermogravimetric (TGA, upper curves) and heat flow (DSC, lower curves) signals for neat AP (black curves) and its mixtures with 5 % $[Pr(BT)(H_2O)_7]_2[BT]{\cdot}6H_2O$ (blue) and 5 % $[Dy(H_2O)_8]_2[BT]_3{\cdot}4H_2O$ (red) at a heating rate of 10 K/min.

Table 4. Catalytic effect of 5,5′-bitetrazolates on AP decomposition and combustion.

Sample	Decomposition		Combustion
	T_{max}^{DTG} [°C]	Δ [°C]	*Z* under a pressure 4 MPa [%]
Pure AP	416	–	–
$[Y_2(BT)_3(H_2O)_{12}]{\cdot}2H_2O$	318	98	1.05
$[Ce_2(BT)_3(H_2O)_{12}]{\cdot}2H_2O$	382	34	0.95
$[Pr(BT)(H_2O)_7]_2[BT]{\cdot}6H_2O$	365	51	1.20
$[Nd(BT)(H_2O)_7]_2[BT]{\cdot}6H_2O$	344	72	0.89
$[Sm(BT)(H_2O)_7]_2[BT]{\cdot}6H_2O$	330	86	0.77
$[Dy(H_2O)_8]_2[BT]_3{\cdot}4H_2O$	321	95	0.79
$[Ho(H_2O)_8]_2[BT]_3{\cdot}4H_2O$	321	95	0.71
$[Er(H_2O)_8]_2[BT]_3{\cdot}4H_2O$	320	96	0.79
$[Yb(H_2O)_8]_2[BT]_3{\cdot}4H_2O$	356	60	1.04

Some of the 5,5′-bitetrazolates (Y, La, Ce, Sm) were added to HMX, but no effect on its decomposition mechanism was observed; this is consistent with the known difficulties in nitramine catalysis.[6,18]

Additionally, the catalytic effects of the lanthanide 5,5′-bitetrazolates on AP combustion were studied. The catalysis of thermal decomposition does not necessarily lead to combustion catalysis.[7a,19] In the abovementioned thermal analysis measurements, the heating rate was 10 K/min, whereas this value approaches 10^4–10^6 K/s in a combustion wave. In the first case, the bound water molecules evolve before the catalytic decomposition occurs; however, during combustion tests, this process is superimposed with the combustion itself, and we can expect the water to have a detrimental effect on the burning rate.[20]

The catalytic efficiency was determined as the ratio (*Z*) of the burning rate of AP with additive to that for the AP monopropellant. The results for the series of 5,5′-bitetrazolates are shown in Table 4. Only the addition of $[Pr(BT)(H_2O)_7]_2[BT]{\cdot}6H_2O$ appreciably (by 20 %) increases the AP burning rate. The addition of yttrium and ytterbium 5,5′-bitetrazolate resulted in ca. 5 % augmentation, which is comparable to the error in the measurement of the *Z* value. The other salts decrease the burning rate of ammonium perchlorate, apparently because of their significant water contents.

3. Conclusion

We completed the $[Ln_2(BT)_3]{\cdot}nH_2O$ series through the addition of the missing examples [M = Pr (**1**), Gd (**2**), Dy (**4**), Ho (**5**), Tm (**6**), Yb (**7**), Lu (**8**), and Y (**3**)] and developed a new procedure for the synthesis of such complexes. Hydrates of the rare-earth 5,5′-bitetrazolates were obtained in good-to-high yields from sodium 5,5′-bitetrazolate and the available rare-earth chlorides, nitrates, or acetates.

The solid-state structures of the new rare-earth complexes with the BT ligand were determined by XRD. Our results confirmed the previous findings by Eulgem et al.[5] that there are three structural types for RE BT complexes: (1) The La and Ce complexes have a $Ln_2(BT)_3$ structural motif with two chelating BT ligands and one bridging BT ligand. (2) The LREEs from Pr to Gd have a Ln(BT) motif with one chelating BT ligand attached to a metal center and a BT ligand in the outer sphere. (3) The more Lewis acidic HREEs Y and Tb to Lu have saltlike structures in which the metal atom is coordinated to eight water molecules, that is, $M(H_2O)_8$ with all BT^{2-} ions in the outer sphere.

Luminescence spectroscopy revealed the presence of simultaneous sensitization and back-metal-to-ligand energy transfer, which resulted in low luminescence intensities, and the luminescence intensity is additionally decreased through quenching by the water molecules. At the same time, the luminescence spectroscopy data demonstrated its sensitivity for the determination of the number of coordinated water molecules, even for solid samples.

When the investigated salts were heated, they exhibited mass loss in three stages. For the first stage corresponding to dehydration, a correlation between the characteristic temperature, that is, the strength of water bonding, and the atomic number of the lanthanide cation was established.

5,5′-Bitetrazolates are active catalysts for the thermolysis of ammonium perchlorate and reduce its decomposition temperature by ca. 100 °C. During the combustion process, the negative effect from the evolved water apparently outweighs the catalytic effect of the metal formed. An augmentation of the burning rate (by 20 %) of ammonium perchlorate monopropellant was revealed only for the Pr compound.

4. Experimental Section

4.1 General Remarks

Caution! Preparations including KCN and NaN_3 in acidic media are extremely dangerous owing to the formation of volatile HCN and explosive HN_3 and should be performed in an appropriate hood.

The elemental analyses were performed with an Elementar Vario MICRO cube apparatus. The thermal stabilities were studied with a DSC/TG thermal analyzer (STA449 F3, Netzsch). Samples (ca. 1 mg) in a closed alumina pan with a pierced lid were heated to 550 °C at a rate 10 K/min under an argon flow (70 mL/min). The burning rates were measured during combustion in a constant-pressure bomb through high-speed video recording at an initial pressure of 4 MPa, which is higher that the low-pressure limit of AP of ca. 2 MPa.[5,13] Cylindrical samples were pressed in charges of 6 mm diameter. The emission and excitation spectra were measured with a Fluorolog 3 spectrofluorometer with excitation with a xenon lamp. The luminescence lifetime measurements were performed with the same system. All of the luminescence decay curves were perfect single-exponential functions.

4.2 X-ray Crystallographic Studies

The single-crystal X-ray diffraction data for **1**–**8** were recorded with a Bruker APEX-II CCD diffractometer (graphite monochromator, ω and φ scanning mode) and corrected for absorption with the SADABS program.[21] For details, see Table 1. The structures were determined by direct methods and refined by full-matrix least-squares techniques on F^2 in an anisotropic approximation for non-hydrogen atoms. The hydrogen atoms of the water molecules were objectively localized in the difference-Fourier map and included in the refinement in a riding model with isotropic displacement parameters [U_{iso}(H) = 1.5U_{eq}(O)]. All calculations were performed with the SHELXTL program suite.[22]

CCDC 1559654 (for **1**), 1559655 (for **2**), 1559656 (for **3**), 1559657 (for **4**), 1559658 (for **5**), 1559659 (for **6**), 1559660 (for **7**), and 1559661 (for **8**) contain the supplementary crystallographic data for this paper. These data can be obtained free of charge from The Cambridge Crystallographic Data Centre.

4.3 Synthetic Procedures

4.3.1 Manganese(II) 5,5′-Bitetrazolate:[23] A round-bottomed flask equipped with a reflux condenser and a magnetic stir bar was charged with NaN_3 (13.00 g, 0.2 mol, 1.6 equiv.), KCN (13.02 g, 0.2 mol, 1.6 equiv.), and deionized water (120 mL). The reaction mixture was cooled to 0 °C, and MnO_2 (10.95 g, 0.126 mol) was added in small portions followed by the dropwise addition of a solution of $CuSO_4{\cdot}5H_2O$ (0.4 g, 2.51 mmol) in a mixture of H_2SO_4 (15 mL, 20 g), glacial acetic acid (15 mL, 16 g), and deionized water (50 mL). During the addition of the MnO_2, $CuSO_4{\cdot}5H_2O$, H_2SO_4, and acetic acid, the temperature of the reaction mixture was maintained below 15 °C. After that, the reaction mixture was heated to 80 °C for 3 h and then cooled to room temperature. The reaction mixture was filtered, and the solid was washed with deionized water (3 × 30 mL) and air-dried to give crude manganese 5,5′-bitetrazolate as a brown solid (19.5 g, 89 %).

4.3.2 Disodium 5,5′-Bitetrazolate Pentahydrate:[24] A round-bottomed flask equipped with a reflux condenser and a magnetic stir bar was charged with manganese 5,5′-bitetrazolate (19.5 g, 0.102 mol) and sodium carbonate (11.0 g, 0.104 mol) suspended in deionized water (155 mL), and the mixture was heated under reflux for 1.5 h. The reaction mixture was cooled to room temperature and filtered, and the solid residue was washed with boiling water (20 mL). The filtrates were combined and concentrated in vacuo until crystallization started. The solution was heated until all of the solids dissolved and then slowly cooled to 5 °C. After 2 d, the resulting light-green crystals were collected by filtration and recrystallized from the minimum amount of boiling water. Filtration provided disodium 5,5′-bitetrazolatepentahydrate as colorless needles (15.73 g, 64 %). $C_2H_{10}N_8Na_2O_5$ (272.13 g mol^{-1}): calcd. C 8.83, H 3.70, N 41.18; found C 8.99, H 3.53, N 40.87. ^{13}C NMR (151 MHz, D_2O): δ = 154.5 ppm.[5]

4.3.3 General Procedure for the Synthesis of Rare-Earth 5,5′-Bitetrazolate Hydrates 1–8: To a solution of disodium 5,5′-bitetrazolate pentahydrate (300 mg, 1.10 mmol) in deionized water (ca. 7 mL) was added a solution of the corresponding rare-earth salt in a minimal amount of water (ca. 7 mL). The reaction mixture was heated until a clear solution was obtained and then cooled slowly to 5 °C. If the heating of the reaction mixture caused the formation of a turbid solution, the mixture was filtered, and the hot clear solution was left for crystallization. After 2 d at 5 °C, the precipitate was collected by filtration and air-dried to give crystals of the rare-earth 5,5′-bitetrazolate hydrates. By this general procedure, the Y and Ln complexes were obtained.

$[La_2(BT)_3(H_2O)_{12}]{\cdot}2H_2O$ was obtained from $LaCl_3{\cdot}7H_2O$ (273 mg, 0.73 mmol) as a colorless solid in 74 % yield. ^{13}C{^{1}H} NMR (151 MHz, D_2O): δ = 154.2 ppm.

$[Ce_2(BT)_3(H_2O)_{12}]{\cdot}2H_2O$ was obtained from $CeCl_3{\cdot}7H_2O$ (274 mg, 0.73 mmol) as a colorless solid in 71 % yield.

$[Pr(BT)(H_2O)_7]_2[BT]{\cdot}6H_2O$ (**1**) was obtained from $Pr(NO_3)_3{\cdot}6H_2O$ (320 mg, 0.73 mmol) as a light-green solid in 79 % yield. $C_6H_{40}N_{24}O_{20}Pr_2$ (1050.35):calcd. C 6.86, H 3.84, N 32.00; found C 6.99, H 3.65, N 31.76.

$[Nd(BT)(H_2O)_7]_2[BT]{\cdot}6H_2O$ was obtained from $Nd(NO_3)_3{\cdot}6H_2O$ (322 mg, 0.73 mmol) as a purple solid in 80 % yield. ^{13}C{^{1}H} NMR (151 MHz, [D$_6$]DMSO): δ = 158.2 ppm.

$[Sm(BT)(H_2O)_7]_2[BT]{\cdot}6H_2O$ was obtained from $Sm(NO_3)_3{\cdot}6H_2O$ (327 mg, 0.73 mmol) as a light-yellow solid in 69 % yield.

$[Eu(BT)(H_2O)_7]_2[BT]{\cdot}6H_2O$ was obtained from $Eu(OAc)_3{\cdot}3H_2O$ (251 mg, 0.73 mmol) as a colorless solid in 67 % yield.

$[Gd(BT)(H_2O)_7]_2[BT]{\cdot}6H_2O$ (**2**) was obtained from $GdCl_3{\cdot}6H_2O$ (327 mg, 0.73 mmol) as a colorless solid in 72 % yield. $C_6H_{40}Gd_2N_{24}O_{20}$ (1083.03): calcd. C 6.65, H 3.72, N 31.04; found C 6.84, H 3.84, N 31.41.

$[Y(H_2O)_8]_2[BT]_3{\cdot}4H_2O$ (**3**) was obtained from $YCl_3{\cdot}6H_2O$ (223 mg, 0.73 mmol) as a colorless solid in 68 % yield. $C_6H_{40}N_{24}O_{20}Y_2$ (946.34): calcd. C 7.62, H 4.26, N 35.52; found C 7.77, H 4.30, N 35.48. DSC/TGA (10 K min^{-1}): 105.5 °C (dehydration, endothermic), 166.3 °C (dehydration, endothermic), 333.8 °C (decomposition, exothermic). ^{13}C{^{1}H} NMR (151 MHz, D_2O): δ = 154.3 ppm.

$[Tb(H_2O)_8]_2[BT]_3{\cdot}4H_2O$ was obtained from $Tb(NO_3)_3{\cdot}6H_2O$ (333 mg, 0.73 mmol) as a colorless solid in 73 % yield.

$[Dy(H_2O)_8]_2[BT]_3{\cdot}4H_2O$ (**4**) was obtained from $Dy(NO_3)_3{\cdot}5H_2O$ (333 mg, 0.73 mmol) as a colorless solid in 75 % yield. $C_6H_{40}Dy_2N_{24}O_{20}$ (1093.53): calcd. C 6.59, H 3.69, N 30.74; found C 6.55, H 3.78, N 30.89.

$[Ho(H_2O)_8]_2[BT]_3{\cdot}4H_2O$ (**5**) was obtained from $Ho(NO_3)_3{\cdot}5H_2O$ (324 mg, 0.73 mmol) as a pink solid in 73 % yield. $C_6H_{40}Ho_2N_{24}O_{20}$ (1098.39): calcd. C 6.56, H 3.67, N 30.60; found C 6.73, H 3.68, N 30.73.

$[Er(H_2O)_8]_2[BT]_3{\cdot}4H_2O$ was obtained from $Er(NO_3)_3{\cdot}5H_2O$ (326 mg, 0.73 mmol) as a light pink solid in 81 % yield.

$[Tm(H_2O)_8]_2[BT]_3{\cdot}4H_2O$ (**6**) was obtained from $Tm(NO_3)_3{\cdot}5H_2O$ (327 mg, 0.73 mmol) as a colorless solid in 66 % yield. $C_6H_{40}N_{24}O_{20}Tm_2$ (1106.40): calcd. C 6.51, H 3.64, N 30.38; found C 6.60, H 3.68, N 30.31.

$[Yb(H_2O)_8]_2[BT]_3{\cdot}4H_2O$ (**7**) was obtained from $Yb(NO_3)_3{\cdot}5H_2O$ (330 mg, 0.73 mmol) as a colorless solid in 81 % yield.

$C_6H_{40}N_{24}O_{20}Yb_2$ (1114.64): calcd. C 6.47, H 3.62, N 30.16; found C 6.52, H 3.66, N 30.14.

$[Lu(H_2O)_8]_2[BT]_3{\cdot}4H_2O$ (**8**) was obtained from $Lu(NO_3)_3{\cdot}6H_2O$ (345 mg, 0.73 mmol) as a colorless solid in 74 % yield. $C_6H_{40}Lu_2N_{24}O_{20}$ (1118.46): calcd. C 6.44, H 3.60, N 30.06; found C 6.52, H 3.60, N 29.75.

4.3.4 General Procedure for the Synthesis of Rare-Earth 5,5′-Bitetrazolate Deuterates: Disodium 5,5′-bitetrazolate pentahydrate (0.300 g, 1.10 mmol) and the corresponding RE salt (0.73 mmol) were separately dissolved in D_2O (5 mL each), and then the solutions were evaporated to dryness. This dissolution–evaporation cycle was repeated three times for each reagent. Then, solutions of each reagent in D_2O (ca. 7 mL) were prepared and combined. The resulting solution was kept at 5 °C for 2 d. The crystals formed were collected by filtration and air-dried to give rare-earth 5,5′-bitetrazolate deuterates.

$[Eu(BT)(D_2O)_7]_2[BT]{\cdot}6D_2O$ was obtained from $Eu(OAc)_3{\cdot}3H_2O$ (251 mg, 0.73 mmol) as a colorless solid in 68 % yield.

$[Tb(D_2O)_8]_2[BT]_3{\cdot}4D_2O$ was obtained $Tb(NO_3)_3{\cdot}6H_2O$ (from 333 mg, 0.73 mmol) as a colorless solid in 72 % yield.

Acknowledgments

This study was financially supported in part by the Ministry of Education and Science of the Russian Federation (Agreement number 02.a03.21.0008). This work was done by M. A. Topchiy, A. F. Asachenko, and M. S. Nechaev as part of the A. V. Topchiev Institute of Petrochemical Synthesis (TIPS) Russian Academy of Sciences (RAS) State Plan.

Keywords: Rare earths · Nitrogen heterocycles · Luminescence · Combustion catalysis

[1] a) A. Hammerl, M. A. Hiskey, G. Holl, T. M. Klapötke, K. Polborn, R. Stierstorfer, J. J. Weigand, *Chem. Mater.* **2005**, *17*, 3784–3793; b) R. P. Singh, R. D. Verma, D. T. Meshri, J. M. Shreeve, *Angew. Chem. Int. Ed.* **2006**, *45*, 3584–3601; *Angew. Chem.* **2006**, *118*, 3664; c) C. F. Ye, H. X. Gao, J. A. Boatz, G. W. Drake, B. Twamley, J. M. Shreeve, *Angew. Chem. Int. Ed.* **2006**, *45*, 7262–7265; *Angew. Chem.* **2006**, *118*, 7420; d) H. X. Gao, C. F. Ye, C. M. Piekarski, J. M. Shreeve, *J. Phys. Chem. C* **2007**, *111*, 10718–10731; e) N. Fischer, D. Izsak, T. M. Klapötke, S. Rappengluck, J. Stierstorfer, *Chem. Eur. J.* **2012**, *18*, 4051–4062; f) S. H. Li, Y. Wang, C. Qi, X. X. Zhao, J. C. Zhang, S. W. Zhang, S. P. Pang, *Angew. Chem. Int. Ed.* **2013**, *52*, 14031–14035; *Angew. Chem.* **2013**, *125*, 14281; g) X. Y. Liu, W. J. Gao, P. P. Sun, Z. Y. Su, S. P. Chen, Q. Wei, G. Xie, S. L. Gao, *Green Chem.* **2015**, *17*, 831–836; h) S. Zhang, Q. Yang, X. Y. Liu, X. N. Qu, Q. Wei, G. Xie, S. P. Chen, S. L. Gao, *Coord. Chem. Rev.* **2016**, *307*, 292–312.

[2] a) A. Hammerl, G. Holl, T. M. Klapötke, P. Mayer, H. Noth, H. Piotrowski, M. Warchhold, *Eur. J. Inorg. Chem.* **2002**, *2002*, 834–845; b) K. F. Warner, R. H. Granholm, *J. Energ. Mater.* **2011**, *29*, 1–6.

[3] a) J. Rocha, L. D. Carlos, F. A. A. Paz, D. Ananias, *Chem. Soc. Rev.* **2011**, *40*, 926–940; b) J. C. G. Bünzli, *Coord. Chem. Rev.* **2015**, *293*, 19–47.

[4] J. C. G. Bünzli, *Chem. Rev.* **2010**, *110*, 2729–2755.

[5] P. J. Eulgem, A. Klein, N. Maggiarosa, D. Naumann, R. W. H. Pohl, *Chem. Eur. J.* **2008**, *14*, 3727–3736.

[6] D. J. G. Lengelle, J. F. Trubert in *Progress in Astronautics and Aeronautics, Vol. 185* (Eds.: V. Yang, T. B. Brill, W. Z. Ren), AIAA, Reston, **2000**, pp. 287–334.

[7] a) A. P. Glazkova, *Catalysis of the Combustion of Explosives [in Russian]*, Nauka, Moscow, **1976**; b) K. Kishore, M. R. Sunitha, *AIAA J.* **1979**, *17*, 1118–1125; c) K. Kreitz, E. Petersen, D. Reid, S. Seal in *49th AIAA Aerospace Sciences Meeting including the New Horizons Forum and Aerospace Exposition*, American Institute of Aeronautics and Astronautics, **2011**; d) V. P. Sinditskii, A. N. Chernyi, D. A. Marchenkov, *Combust. Explos. Shock Waves (Engl. Transl.)* **2014**, *50*, 158–167; e) S. Isert, L. J. Groven, R. P. Lucht, S. F. Son, *Combust. Flame* **2015**, *162*, 1821–1828.

[8] N. Kubota, *Propellants and Explosives: Thermochemical Aspects of Combustion*, Wiley-VCH, Weinheim, **2007**, p. 245.

[9] D. Chen, S. L. Huang, Q. Zhang, Q. Yu, X. Q. Zhou, H. Z. Li, J. S. Li, *RSC Adv.* **2015**, *5*, 32872–32879.

[10] D. W. Smith, *J. Chem. Educ.* **1977**, *54*, 540–541.

[11] Y. Marcus, *J. Chem. Soc. Faraday Trans. 1* **1987**, *83*, 339–349.

[12] M. E. Essington, *Soil and Water Chemistry: An Integrative Approach*, 2nd ed., CRC Press, Boca Raton, FL, **2015**.

[13] C. Huang, Z. Bian in *Rare Earth Coordination Chemistry* (Ed.: C. Huang), John Wiley & Sons, Singapore, **2010**, pp. 1–39.

[14] M. Albin, W. D. Horrocks, *Inorg. Chem.* **1985**, *24*, 895–900.

[15] V. V. Utochnikova, N. N. Solodukhin, A. A. Aslandukov, K. V. Zaitsev, A. S. Kalyakina, A. A. Averin, I. A. Ananyev, A. V. Churakov, N. P. Kuzmina, *Eur. J. Inorg. Chem.* **2017**, 107–114.

[16] *NATO Standardization Agreement (STANAG) on Explosives, Friction Sensitivity Tests, No. 4487, Ed. 1*, **2002**.

[17] V. V. Boldyrev, *Thermochim. Acta* **2006**, *443*, 1–36.

[18] F. S. Blomshield, *Report NWC-TP-6992*, Naval Weapons Center Report, **1989**.

[19] K. J. Kraeutle in *Proc. 18th JANNAF Combustion Meeting, Vol. 2*, **1981**, pp. 383–394.

[20] A. I. Atwood, K. P. Ford, C. J. Wheeler, *Prog. Propul. Phys.* **2013**, *4*, 3–14.

[21] G. M. Sheldrick, *Bruker AXS*, Madison, WI, **2003**.

[22] G. M. Sheldrick, *Acta Crystallogr., Sect. C: Struct. Chem.* **2015**, *71*, 3–8.

[23] J. H. Nelson, N. E. Takach, R. A. Henry, D. W. Moore, W. M. Tolles, G. A. Gray, *Magn. Reson. Chem.* **1986**, *24*, 984–994.

[24] L. H. Finger, F. G. Schroder, J. Sundermeyer, *Z. Anorg. Allg. Chem.* **2013**, *639*, 1140–1152.

Received: September 28, 2017